

# Adaptive Resolution Molecular Dynamics Simulation: Changing the Degrees of Freedom on the Fly

Matej Praprotnik,\* Luigi Delle Site, and Kurt Kremer

*Max-Planck-Institut für Polymerforschung, Ackermannweg 10, D-55128 Mainz, Germany*

(Dated: August 14, 2018)

We present a new adaptive resolution technique for efficient particle-based multiscale molecular dynamics (MD) simulations. The presented approach is tailor-made for molecular systems where atomistic resolution is required only in spatially localized domains whereas a lower mesoscopic level of detail is sufficient for the rest of the system. Our method allows an on-the-fly interchange between a given molecule's atomic and coarse-grained level of description, enabling us to reach large length and time scales while spatially retaining atomistic details of the system. The new approach is tested on a model system of a liquid of tetrahedral molecules. The simulation box is divided into two regions: one containing only atomistically resolved tetrahedral molecules, the other containing only one particle coarse-grained spherical molecules. The molecules can freely move between the two regions while changing their level of resolution accordingly. The coarse-grained and the atomistically resolved systems have the same statistical properties at the same physical conditions.

## I. INTRODUCTION

Many problems in complex soft matter systems are inherently multiscale in nature, i.e., microscopic interactions are coupled strongly to meso- and macroscopic properties. Despite the increasing computational power and ongoing efforts to enhance the efficiency of molecular dynamics (MD) integration algorithms[1, 2, 3, 4, 5, 6], all-atom MD simulations are often incapable to cover the time and length scales needed in order to reach relaxation in a typical molecular system, such as a polymer solution or melt. In many cases it is also questionable, whether the huge amount of detail information might not even obscure the relevant structural information. On the other hand, details of the chemistry do not affect universal power laws but the prefactors of these power laws, which can vary by several orders of magnitude themselves. Thus even on the more coarse-grained level it is advisable to keep a link to the specific chemistry under investigation[7, 8]. In addition typical soft matter systems can be quite inhomogeneous in a way, that different regions within one system are sufficiently described by more or less detail. A consistent and at the same time highly efficient ansatz to understand modern soft matter systems (both of synthetic as well as biological origin) has to take such considerations into account. One first way to tackle this, was to reduce the number of de-

grees of freedom by a systematic coarse-graining, which retains only those degrees of freedom that are relevant for the particular property of interest. Examples of molecular systems where the coarse-graining approach has been used with much success are fluids[9], lipid bilayers [10, 11, 12, 13, 14], and polymer systems[15, 16, 17, 18].

Since some specific chemical details are usually lost in the coarse-graining procedure, much effort has been devoted recently to the development of multiscale modeling approaches, where different parts of the system are modeled at different levels of detail to account for the local resolution requirement[19, 20, 21, 22, 23, 24]. In the dual-resolution modeling approach for studying the behavior of polymers near metal surfaces[22, 23, 24], for example, polymer chain ends that interact with the metal surface are represented partially atomistically while the remaining parts of the polymers, where lower resolution is adequate, are represented as bead-spring chains. However, the switching between different levels of resolution, i.e, the atomic and mesoscopic, is not allowed during the course of that MD simulation, and therefore the initial level of detail and thereby the number of degrees of freedom in the system remain unchanged. Since the chain ends that interact with the metal typically remain close to the surface and they only contain a small fraction of the whole system, an adaptive on-the-fly change of the molecules' resolution is not strictly required for this class of systems. Another approach reported in the literature concerns the link between quantum mechanical and classical MD simulations. In this QM/MM approach a small subset of the system is defined and considered as quantum mechanical, while the rest is

---

\*On leave from National Institute of Chemistry, Hajdrihova 19, 1000 Ljubljana, Slovenia. Electronic Mail: praprot@cmm.ki.si.

treated by a classical force field simulation. Here the atoms as well as the regions of the different regimes are fixed from the very beginning [25], restricting the application to rather specific cases.

In contrast, MD simulations, in which the spatially localized atomistic domains frequently exchange particles with the remaining mesoscopic part of the system, would allow for much wider applications. Then it would be possible to define certain areas or develop criteria for certain situations, which ask for a more detailed view, while the rest of the system can be treated on the more coarse-grained level. It is the purpose of this paper to present a first attempt of an MD simulation of that kind. Because of that we here at first restrict ourselves to a most elementary model system. Of course one also could resort to Monte Carlo simulations, where different levels of detail are combined. This actually would be somewhat simpler because of the purely stochastic nature of this simulation method. Since we are eventually aiming at molecular systems, where collective motions are crucial, we decided to stick to the MD approach. Existing hybrid MD methods that concurrently couple different length scales have been developed to study solid state systems, where atomistic MD was either combined with the finite elements method[26, 27, 28] or it was linked to a quantum mechanical model[29]. To our knowledge, however, in pursuit of this objective no adaptive hybrid atomistic/mesoscale particle-based MD method, which would allow to dynamically adjust the level of detail, which means the adjustment of the degrees of freedom in the system, has been developed so far.

In this paper we present a novel adaptive resolution MD scheme that combines a full atomistic description of a desired region of the system with a mesoscale treatment of the remaining part. The key feature of the new method is that it allows to dynamically adapt the level of a given molecule's resolution according to its position in the system. Hence, the number of degrees of freedom is not a conserved quantity in our MD simulations. Furthermore, the presented method is not restricted to couple only the atomistic and mesoscopic levels of detail but can also be applied to systems with mesoscopic domains that are described at different levels of coarse-graining. Here we present a first test case, showing that such an approach is feasible. Therefore the new approach is tested for a simple model liquid consisting of tetrahedral molecules. The simulation box is divided into two regions: one containing "atomistically"

resolved tetrahedral molecules, the other containing coarse-grained spherical molecules. Molecules are allowed to freely move between the two regions while changing their level of resolution accordingly. The results show that the statistical properties of the corresponding fully atomistic system are accurately reproduced by using the proposed hybrid scheme. In particular, gradients in the chemical potential across the artificial interface where the resolution changes and corresponding spurious fluxes can be avoided. Although we applied the new method here to a generic test system it should find application in more realistic physical systems. There has been an initial attempt reported in Ref. [30], where MD simulation of an inhomogeneously coarse-grained system of liquid methane has been described. There the starting point were two established models for methane, a five site atomistic and a one site spherical where the interaction between molecules of different species was derived by standard Lennard-Jones mixing rules with the hydrogens of the atomistic invisible to the spherical molecules. In this case it turned out that an effective flux between the two different regimes occurred. This effect is partially due to the different equilibrium state points described by the two models, but in any case in that approach no effective potential between coarse-grained molecules was derived. Our approach differs from that since here we derive such potentials in such a way that the two regimes are in true thermodynamic equilibrium.

The organization of the article is as follows. In section 2 the methodology is presented, whereby in the first step a coarse-grained model is derived and parameterized from a fully atomistic system and then, in the second step, the atomic and mesoscopic length scales are systematically coupled in a hybrid atomistic/mesoscopic model. The computational details are given in section 3. The results and discussion are presented in section 4, followed by conclusions in section 5.

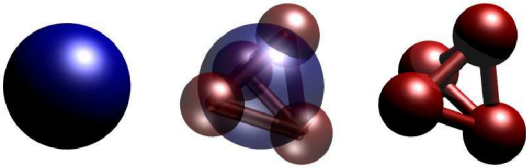
## II. METHODOLOGY

In this section, the model systems are described and the methodology for the adaptive multiscale MD simulations is presented.

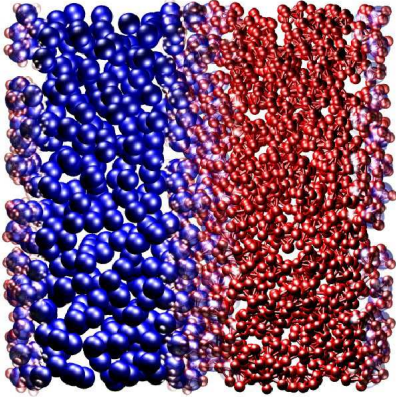
## Models

### All-Atom Model

First, we introduce our reference explicit all-atom (*ex*) model. Consider a system of  $n$  tetrahedral molecules consisting of  $N = 4$  atoms of the same mass  $m_0$  connected by anharmonic bonds as presented in figure 1 (a) (consider only the right red molecule).



(a)



(b)

FIG. 1: (a) The on-the-fly interchange between the atomic and coarse-grained levels of description. The middle hybrid molecule is a linear combination of fully atomistic tetrahedral molecule with an additional center of mass particle representing the coarse-grained molecule. (b) Snapshot of the hybrid atomistic/mesoscopic model at  $\rho^* = 0.1$  and  $T^* = 1$  (LJ units). The red molecules are the explicit atomistically resolved tetrahedral molecules, the blue molecules are the corresponding one particle coarse-grained molecules.

All atoms in the system interact according to a purely repulsive shifted 12-6 Lennard-Jones potential with a cutoff at  $2^{1/6}\sigma$ :

$$U_{LJ}^{atom}(r_{i\alpha j\beta}) = \begin{cases} 4\epsilon\left[\left(\frac{\sigma}{r_{i\alpha j\beta}}\right)^{12} - \left(\frac{\sigma}{r_{i\alpha j\beta}}\right)^6 + \frac{1}{4}\right]; & r_{i\alpha j\beta} \leq 2^{1/6}\sigma \\ 0; & r_{i\alpha j\beta} > 2^{1/6}\sigma \end{cases} \quad (1)$$

where  $r_{i\alpha j\beta}$  is the distance between the atom  $i\alpha$  of the molecule  $\alpha$  and the atom  $j\beta$  of the molecule  $\beta$ . We use  $\epsilon$  as a unit of energy. All atoms have the same excluded volume diameter  $\sigma$ , where  $\sigma$  is the unit of length. The neighboring atoms in a given molecule  $\alpha$  are linked via an attractive FENE potential

$$U_{FENE}^{atom}(r_{i\alpha j\alpha}) = \begin{cases} -\frac{1}{2}kR_0^2 \ln\left[1 - \left(\frac{r_{i\alpha j\alpha}}{R_0}\right)^2\right]; & r_{i\alpha j\alpha} \leq R_0 \\ \infty; & r_{i\alpha j\alpha} > R_0 \end{cases} \quad (2)$$

with divergence length  $R_0 = 1.5\sigma$  and stiffness  $k = 30\epsilon/\sigma^2$ , so that the average bond length is approximately  $1.0\sigma$  for  $k_B T = \epsilon$ , where  $T$  is the temperature of the system and  $k_B$  is Boltzmann's constant. The functional form of these potentials and their parameters are the same as usually employed in polymer MD simulations[15].

### Coarse-Grained Model

Next, we map the atomistic model to a coarse-grained (*cg*) mesoscopic model. For the latter we have chosen a system composed of  $n$  one-particle molecules schematically depicted in figure 1 (a) (consider only the left blue molecule). A given coarse-grained molecule  $\alpha$  in the system has a mass  $M_\alpha = 4m_0$  equal to the total mass of the explicit tetrahedral molecule. All rotational and vibrational degrees of freedom of atomistically resolved tetrahedral molecules are thus removed, and the number of nonbonded interactions is strongly decreased as well.

We shall now find an effective pair potential between coarse-grained molecules such that the structural properties of the underlying atomistic model are reproduced. There is usually no unique way to coarse-grain to an effective pair potential, which is in general temperature and density dependent [31, 32, 33], just as in statistical mechanics there are different ways to perform a renormalization group step. Here, we extract the effective pair

potential from a center-of-mass radial distribution function ( $\text{RDF}_{cm}$ ) of the reference atomistic model using the potential of mean force  $PMF(r)$  as

$$U^{cm}(r) \approx PMF(r) = -k_B T \log g_{ex}^{cm}(r), \quad (3)$$

where  $g_{ex}^{cm}(r)$  is the  $\text{RDF}_{cm}$  of the all-atom system and  $U^{cm}(r)$  is the derived effective pair potential[34]. The effective potential obtained in this way is correct only in the limit of zero density, where the many-body contributions vanish. For systems with nonzero densities in principle many-body interactions would be needed just as for the classical renormalization group theory in statistical mechanics. In a similar spirit we here resort to the (expected) relevant part in order to gain a significant speed up in our simulations. Because of that we use the PMF as the initial guess for the effective pair potential in systems with nonzero density. Then this is further fine-tuned until the  $\text{RDF}_{cm}$ s and pressures of the reference atomistic and coarse-grained systems match[34]. As it turns out (see the Results and Discussion section) the effective pair potential acting between our coarse-grained molecules is significantly softer than the pair potential between atoms of the resolved molecules in accordance with the results previously found in the literature[33, 35].

*Transition Regime: Hybrid Atomistic/Mesoscopic Model*

Let us now introduce a hybrid explicit/coarse-grained (*ex-cg*) model. Consider a box of  $n$  molecules where one half of the box is occupied by atomistically resolved four-atom tetrahedral molecules while the other half is filled up with the same number of corresponding coarse-grained one-particle molecules as schematically presented in figure 1 (b). The two domains exchange molecules which adapt their level of resolution accordingly. To ensure that the transition between the two different levels of description is smooth, i.e., the rotational and vibrational degrees of freedom of a given molecule are gradually 'switched on/off' as it crosses the boundary between the atomistic and coarse-grained domains, we also introduce an interface layer for handshaking between atomistic and mesoscale regions. In this regime also the rotational and vibrational velocities have to be reintroduced in a consistent way. Due to the periodic boundary conditions employed in our simulations there are in fact two such layers as depicted in figure 1 (b).

Since the total number of molecules  $n$  in the system is a conserved quantity in our constant temperature simulations, we sample the phase space from the  $nVT$  ensemble. However, the total number of degrees of freedom is not constant in this model.

An alternative way compared to the similarities with renormalization group methods, which probably describes the situation even better, is the comparison to a first order phase transition. The rotational and vibrational part of the free energy then can be viewed as the latent heat at this transition. At equilibrium, conditions analogous to two phase coexistence,

$$\mu_{ex} = \mu_{cg}, \quad p_{ex} = p_{cg}, \quad T_{ex} = T_{cg}, \quad (4)$$

must be automatically satisfied, where  $\mu_{ex}$ ,  $p_{ex}$ ,  $T_{ex}$  and  $\mu_{cg}$ ,  $p_{cg}$ ,  $T_{cg}$  are the chemical potentials, pressures, and temperatures of the liquid in the atomistic and coarse-grained domains, respectively. These conditions (4) assure that there is no net flux of molecules between the atomistic and coarse-grained regions. To keep this absolute requirement also then defines a central task. This guarantees that the liquid is homogeneous across the box as it is in the reference fully atomistic system. From a molecular point of view, the artificial resolution boundary must be essentially invisible, i.e., the molecules have to cross the border without experiencing any 'barrier'. Our approach to reach this objective is presented in the proceeding subsection.

### Adaptive Resolution Scheme

To allow a coarse-grained molecule to find an energetically permissible orientation with respect to its neighboring molecules (when it leaves the coarse-grained domain and is remapped into the atomistically resolved four-atom tetrahedral molecule) we introduce an interface layer between the atomistic and coarse-grained regions, which contains 'hybrid' molecules as presented in figure 1. Each hybrid molecule schematically shown in figure 1(a) (consider the middle molecule) is composed of a tetrahedral molecule with an additional massless center-of-mass particle serving as an interaction site. This is similar to the flexible TIP4P water model[36] where apart from the interaction sites on the three atoms of a water molecule an additional interaction site is introduced along the symmetry axis between the hydrogen and oxygen atoms.

Thus, each time a coarse-grained molecule  $\alpha$  leaves that domain and enters the interface layer, it is remapped first into a hybrid molecule with the same center-of-mass position and a random orientation in space, where the relative positions of the tetrahedral atoms are taken from a molecular configuration corresponding to a randomly chosen molecule from the atomistic regime. Each of the four explicit tetrahedral atoms in the hybrid molecule gains at this remapping a velocity equal to the velocity of the corresponding coarse-grained molecule to maintain the linear momentum of the molecule. In addition, the tetrahedral atoms are also assigned rotational/vibrational velocities corresponding to atoms of a random molecule from the atomistic region, where we subtract the total linear momentum of the latter molecule. In this way we ensure that the kinetic energy is distributed among all degrees of freedom according to the equipartition principle as  $k_B T/2$  of average kinetic energy per quadratic degree of freedom while retaining the linear momentum of the coarse-grained molecule. The center-of-mass interaction site moves obeying the constraints:

$$\mathbf{R}_\alpha = \frac{\sum_{i\alpha} m_{i\alpha} \mathbf{r}_{i\alpha}}{M_\alpha}, \quad (5)$$

$$\mathbf{V}_\alpha = \frac{\sum_{i\alpha} m_{i\alpha} \mathbf{v}_{i\alpha}}{M_\alpha}, \quad (6)$$

where  $\mathbf{R}_\alpha$  is a center of mass of the molecule  $\alpha$ ,  $\mathbf{r}_{i\alpha}$  is the position vector of the explicit tetrahedral atom  $i\alpha$  in the molecule  $\alpha$ ,  $\mathbf{V}_\alpha$  is the center-of-mass velocity of the molecule  $\alpha$ ,  $\mathbf{v}_{i\alpha}$  is the velocity of the explicit tetrahedral atom  $i\alpha$ , and  $M_\alpha = \sum_{i\alpha} m_{i\alpha}$  is the total mass of the molecule  $\alpha$ . In our case,  $m_{i\alpha} = m_0$  and  $M_\alpha = 4m_0$  for all  $i\alpha = 1, \dots, 4$  and  $\alpha = 1, \dots, n$ . Each time a hybrid molecule crosses the boundary into atomistic regime it is remapped into a four-particle tetrahedral molecule with the four tetrahedral atoms retaining their current velocities and positions. In this model also the explicit tetrahedral molecules have the center-of-mass interaction sites, but only for the interactions with the hybrid and coarse-grained molecules. Of course, deep in the atomistic region, where the atomistically resolved molecules do not interact anymore with the hybrid and coarse-grained molecules the center-of-mass interaction site can be omitted. Every time a four-particle tetrahedral molecule leaves the atomistic region and enters into the transition regime it is mapped into a hybrid molecule with the four tetrahedral atoms retaining instantaneous velocities and positions with the center-of-mass interac-

tion site moving according to Eqs. (5) and (6). Similarly, as a hybrid molecule crosses a boundary to the coarse-grained region it is mapped into a coarse-grained molecule with a velocity equal to the center-of-mass velocity of the hybrid molecule given by Eq. (6).

To couple the atomic and mesoscopic length scales we define in the spirit of thermodynamic perturbation approach[37, 38] the total intermolecular force acting between centers of mass of molecules  $\alpha$  and  $\beta$  as

$$\mathbf{F}_{\alpha\beta} = w(X_\alpha)w(X_\beta)\mathbf{F}_{\alpha\beta}^{atom} + [1 - w(X_\alpha)w(X_\beta)]\mathbf{F}_{\alpha\beta}^{cm}, \quad (7)$$

where

$$\mathbf{F}_{\alpha\beta}^{atom} = \sum_{i\alpha, j\beta} \mathbf{F}_{i\alpha j\beta}^{atom} \quad (8)$$

is the sum of all pair atom interactions between explicit tetrahedral atoms of the molecule  $\alpha$  and explicit tetrahedral atoms of the molecule  $\beta$  and

$$\mathbf{F}_{i\alpha j\beta}^{atom} = -\frac{\partial U^{atom}}{\partial \mathbf{r}_{i\alpha j\beta}}, \quad (9)$$

$$\mathbf{F}_{\alpha\beta}^{cm} = -\frac{\partial U^{cm}}{\partial \mathbf{R}_{\alpha\beta}}. \quad (10)$$

The vector  $\mathbf{r}_{i\alpha j\beta} = \mathbf{r}_{i\alpha} - \mathbf{r}_{j\beta}$  is the relative position vector of atoms  $i\alpha$  and  $j\beta$ ,  $\mathbf{R}_{\alpha\beta} = \mathbf{R}_\alpha - \mathbf{R}_\beta$  is the relative position vector of the centers of mass of the molecules  $\alpha$  and  $\beta$ ,  $X_\alpha$  and  $X_\beta$  are the  $x$  center-of-mass coordinates of the molecules  $\alpha$  and  $\beta$ , respectively, and  $w$  is the weighting function that determines the 'identity' of a given molecule. The weighting function  $w \in [0, 1]$  is defined in such a way that values  $0 < w < 1$  correspond to a hybrid molecule with extreme cases  $w = 1$  and  $w = 0$  corresponding to a four-atom tetrahedral molecule and one-particle coarse-grained molecule, respectively. Hence, as soon as one of the two interacting molecules  $\alpha$  and  $\beta$  is a coarse-grained molecule with no explicit tetrahedral atoms  $w(X_\alpha)w(X_\beta) = 0$  and  $\mathbf{F}_{\alpha\beta} = \mathbf{F}_{\alpha\beta}^{cm}$ .

We propose the following functional form of the weighting function  $w$ :

$$w(x) = \begin{cases} 1; & d < x \leq \frac{a}{2} - d \\ 0; & -\frac{a}{2} + d \leq x < -d \\ \sin^2[\frac{\pi}{4d}(x+d)]; & -d \leq x \leq d \\ \cos^2[\frac{\pi}{4d}(x - \frac{a}{2} + d)]; & \frac{a}{2} - d < x \leq \frac{a}{2} \\ \cos^2[\frac{\pi}{4d}(x + \frac{a}{2} + d)]; & -\frac{a}{2} \leq x < -\frac{a}{2} + d \end{cases} \quad (11)$$

where  $a$  is the box length and  $d$  the half-width of the interface layer. The weighting function  $w$  is shown in figure 2. Our choice, which takes into account the periodic boundary conditions, is a particularly simple way to ensure an interpolation between  $w = 0$  and  $w = 1$  that is monotonic, continuous, differentiable and has zero slope at the boundaries to the atomistic and coarse-grained regions. Apart from these requirements we consider the precise functional form as immaterial.

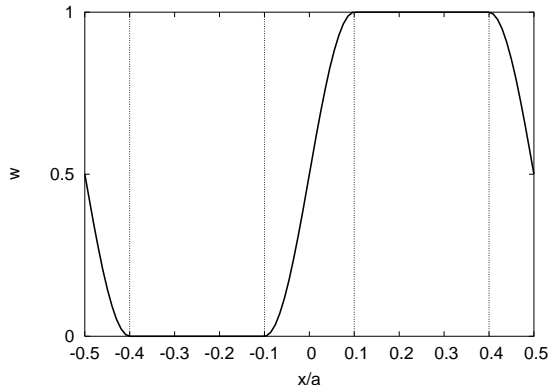


FIG. 2: The weighting function  $w(x) \in [0, 1]$  defined by Eq. (11). The values  $w = 1$  and  $w = 0$  correspond to the atomistic and coarse-grained regions of the hybrid atomistic/mesoscopic system with the box length  $a$ , respectively, while the values  $0 < w < 1$  correspond to the interface layer. Shown is the example where the half-width  $d$  of the interface layer is  $d = a/10$ . The vertical lines denote the boundaries of the interface layers.

Exploiting the analogy with the quantum mechanical mixed state description[39], one can consider a hybrid molecule in the interface layer as a normalized linear combination of a four-atom tetrahedral molecule and a corresponding one-particle coarse-grained molecule. As a given molecule moves from the coarse-grained boundary of the interface layer to the atomistic boundary,  $w$  is gradually changed from 0 to 1 and a coarse-grained molecule with only 3 translational degrees of freedom gradually turns into an atomistically resolved molecule with additional  $3N - 3 = 9$  rotational and vibrational degrees of freedom and a defined spatial orientation. The continuous, i.e., not instantaneous, 'identity' transition is required since a hybrid molecule is given a random orientation at the coarse-grained boundary, and there can consequently be overlaps of its tetrahedral atoms with the atoms of the neighboring molecules. Since at this boundary  $w = 0$  and

the repulsive potential  $U^{atom}$  given in Eq. (1) is capped (see the Computational Details section), the forces acting on these atoms cannot diverge, however. While moving towards the atomistic region the hybrid molecule slowly adapts its orientation via the gradually increasing atomistic interactions with the neighboring molecules. Likewise, as presented in figure 1 (a), as a given molecule moves from the atomistic boundary of the interface layer to the coarse-grained boundary,  $w$  is continuously changing from 1 to 0, the fully atomistically resolved molecule gradually turns into the one particle coarse-grained molecule while omitting all rotational and vibrational degrees of freedom and orientation.

To elucidate the definition of the force calculation in our model we rewrite Eq. (7) as

$$\mathbf{F}_{\alpha\beta} = w(X_\alpha)w(X_\beta)\mathbf{F}_{\alpha\beta}^{atom} + [1 - w(X_\alpha)][1 - w(X_\beta)]\mathbf{F}_{\alpha\beta}^{cm} + [1 - w(X_\alpha)]w(X_\beta)\mathbf{F}_{\alpha\beta}^{cm} + w(X_\alpha)[1 - w(X_\beta)]\mathbf{F}_{\alpha\beta}^{cm}. \quad (12)$$

From Eqs. (8) and (12) one can then deduce that the pair force in Eq. (7) is defined in such a way that two given atoms  $i\alpha$  and  $j\beta$  in given explicit molecules  $\alpha$  and  $\beta$  ( $w(X_\alpha) = 1$  and  $w(X_\beta) = 1$ ) interact via the atomistic potential defined by Eqs. (1) and (2) while two coarse-grained molecules ( $w(X_\alpha) = 0$  and  $w(X_\beta) = 0$ ) interact via the corresponding effective pair potential  $U^{cm}$ . Furthermore, the coarse-grained molecules 'see' the fully atomistically resolved molecules as coarse-grained molecules. Hence, their intermolecular interaction is defined by the effective pair potential  $U^{cm}$ . To ensure that the center-of-mass dynamics governed by Eqs. (5) and (6) of a given explicit or hybrid molecule  $\alpha$  is correct, the total intermolecular force  $\mathbf{F}_{\alpha\beta}^{cm}$  between the atomistically resolved molecule  $\alpha$  and a coarse-grained molecule  $\beta$  is distributed among the explicit atoms of the molecule  $\alpha$  as

$$\mathbf{F}_{i\alpha\beta} = \frac{m_{i\alpha}}{\sum_{i\alpha} m_{i\alpha}} \mathbf{F}_{\alpha\beta}^{cm}, \quad (13)$$

where  $\mathbf{F}_{i\alpha\beta}$  is the force imposed on the explicit tetrahedral atom  $i\alpha$  by the coarse-grained molecule  $\beta$ . The explicit tetrahedral atoms in a given hybrid molecule interact with other explicit atoms in neighboring explicit and hybrid molecules through atomistic forces, while the then massless center-of-mass particle serves as an effective potential interaction site. The total force on a hybrid molecule is then according to Eq. (7) a normalized

linear combination of atomistic and effective pair forces. Using

$$\mathbf{F}_{i\alpha j\beta}^{atom} = -\mathbf{F}_{j\beta i\alpha}^{atom}, \quad (14)$$

$$\mathbf{F}_{\alpha\beta}^{cm} = -\mathbf{F}_{\beta\alpha}^{cm} \quad (15)$$

we obtain from Eq. (7)

$$\mathbf{F}_{\alpha\beta} = -\mathbf{F}_{\beta\alpha}. \quad (16)$$

The force definition in Eq. (7) hence satisfies Newton's Third Law.

Recall that the effective intermolecular potential is determined in such a way that the equations of state for the *ex* and *cg* models match around the state point considered. Therefore, following the scheme, as given by Eq. (7), Eq. (4) is implicitly satisfied, due to which spurious fluxes are avoided at the boundary between the atomistic and coarse-grained regimes.

To summarize, the new adaptive resolution scheme for the hybrid atomistic/mesoscale MD simulations is a two-stage procedure:

1. Derive the effective pair potential  $U^{cm}$  between coarse-grained molecules on the basis of the reference all-atom system.
2. Introduce the interface layer containing the hybrid molecules that have additional interaction sites positioned at their centers of mass. Define a weighting function  $w$  by Eq. (11) and use Eq. (7) for the definition of the intermolecular pair forces. Allow molecules to adapt their level of resolution according to their position in the system as explained in the second paragraph of this subsection.

Finally, since the switching of the resolution can be considered as a first order phase transition, the adaptive resolution scheme must necessarily be employed in combination with a thermostat. Because the latent heat is generated in the transition regime it is important to use a thermostat, which couples locally to the particle motion, e.g., Langevin or Dissipative Particle Dynamics (DPD) thermostats[40].

### III. COMPUTATIONAL DETAILS

#### Temperature Calculation

In order to treat all  $n$  molecules equally regardless of the level of detail, we define, using the

equipartition principle, the temperature of a system only from translational degrees of freedom. The 'translational' temperature

$$T = \frac{2E_k^{cm}}{3nk_B} = \frac{1}{3nk_B} \sum_{\alpha} M_{\alpha} \mathbf{V}_{\alpha}^2, \quad (17)$$

when averaged gives the temperature of the system [41]. Here  $E_k^{cm}$  is the total translational kinetic energy of the system. We also checked the "particle" temperature in the explicit atomistic region. As to be expected we find the same temperature.

#### Pressure Calculation

For the same reason also the pressure calculation is based on the molecular instead of atomic interactions:

$$p = \frac{1}{V} \left[ nk_B T - \frac{1}{3} \sum_{\alpha < \beta} \mathbf{R}_{\alpha\beta} \cdot \mathbf{F}_{\alpha\beta} \right], \quad (18)$$

where  $\mathbf{F}_{\alpha\beta}$  is given by Eqs. (7)[41, 42]. Moreover, using Eq. (18) for pressure evaluation has two additional advantages compared to the pressure calculation based on atomic interactions: first, Eq. (18) is also valid in the case that forces on atoms involve internal non-pairwise-additive contributions, and second, even if all interactions are pairwise additive (as in our case), the pressure calculation based on atomic interactions introduces additional fluctuations in the pressure[42].

#### Multiscale Simulation Details

For computational convenience during the proof-of-principle stage we replace our *ex-cg* model with a model in which the whole box contains exclusively hybrid molecules with four explicit atoms and a center-of-mass interaction site. This has some technical advantages during the tests of the method. The true level of detail of the molecules is then determined from the value of  $w(X_{\alpha})$ . For later large scale, however, of course the original *ex-cg* model composed of the explicit, coarse-grained, and hybrid molecules will be employed. Using Eq. (11) in the replacement model for distinguishing between explicit, coarse-grained, and hybrid molecules of our original *ex-cg* model we can capture all definitions of pair forces for all classes of

particles in our system in a single expression as

$$\begin{aligned} \mathbf{F}_{i\alpha j\beta} = & \\ w(X_\alpha)w(X_\beta)\mathbf{F}_{i\alpha j\beta}^{atom} & + [1 - w(X_\alpha)w(X_\beta)]\delta_{\alpha,\beta}\mathbf{F}_{i\alpha j\beta}^{atom} \\ & + [1 - w(X_\alpha)w(X_\beta)]\frac{m_{i\alpha}m_{j\beta}}{\sum_{i\alpha} m_{i\alpha} \sum_{j\beta} m_{j\beta}}\mathbf{F}_{\alpha\beta}^{cm}, \end{aligned} \quad (19)$$

where  $\mathbf{F}_{i\alpha j\beta}$  is the total pair force between the explicit atom  $i\alpha$  of the molecule  $\alpha$  and the explicit atom  $j\beta$  of the molecule  $\beta$  and  $\delta_{\alpha,\beta}$  is the Kronecker symbol. Summing for  $\alpha \neq \beta$

$$\mathbf{F}_{\alpha\beta} = \sum_{i\alpha, j\beta} \mathbf{F}_{i\alpha j\beta} \quad (20)$$

we regain the total force between molecules  $\alpha$  and  $\beta$  given in Eq. (7). From Eqs. (5), (6), and (19) follows that in the replacement model with only hybrid molecules a hybrid molecule experiences only translational kicks from other molecules in the coarse-grained region ( $w = 0$ ) and hence its center of mass moves exactly as the respective one-particle coarse-grained molecule in the original *ex-cg* model. Similarly, in the explicit region ( $w = 1$ ) a hybrid molecule experiences only atomistic forces and hence its explicit atoms move exactly as the explicit atoms in the respective tetrahedral molecule in the original model. Therefore, the model containing only hybrid molecules interacting via the pair force defined by Eq. (19) together with the applied Langevin thermostat[15] acting on each particle in the system (to assure that the atom velocities are thermalized in accordance with the equipartition principle) exactly mimics the original *ex-cg* model in which the temperature would also be held constant by the Langevin thermostat. From the methodology development point of view, these two models are therefore identical.

This yields the Langevin equation of motion

$$m_i \frac{d^2 \mathbf{r}_i}{dt^2} = \mathbf{F}_i - m_i \Gamma \frac{d\mathbf{r}_i}{dt} + \mathbf{W}_i(t), \quad (21)$$

where  $m_i$  is the mass of particle  $i$ ,  $\mathbf{F}_i$  is the total force acting on the respective particle equal to the sum of pair interactions given by Eq. (19),  $\Gamma$  is the friction constant, and  $\mathbf{W}$  is the random force of a heat bath[43]. We sample the random force from a uniform distribution, since it has been shown that there is no advantage of using Gaussian noise for the Langevin thermostat[44].

The value of the friction constant used in our simulations is  $\Gamma = 0.5\tau^{-1}$  where  $\tau = (\varepsilon/m_0\sigma^2)^{-1/2}$ . The equations of motion are integrated for each particle of the system using

the velocity Verlet algorithm with a  $0.005\tau$  time step. Here, again only for the purpose of testing the method, we use only one time step in the whole system. In the coarse-grained regime actually a significantly larger time step could be used. Therefore ultimately one would like to introduce a multiple time step algorithm. Simulations are performed at temperature  $T = \varepsilon/k_B$  and number density  $\rho = n/V = 0.1/\sigma^3$ . Here  $n = 5001$  is the number of molecules in the system, which can be either the explicit, coarse-grained or hybrid. If we roughly estimate the excluded volume diameter of the coarse-grained molecule  $\sigma_{CG}$  as the distance, where the repulsive effective pair potential between the coarse-grained molecules in our simulations equals  $k_B T$ , i.e.,  $\sigma_{CG} \approx 1.7\sigma$ , then the number density  $\rho = 0.1/\sigma^3 = 0.1(\sigma_{CG}/\sigma)^3/\sigma_{CG}^3 \approx 0.5/\sigma_{CG}^3$  corresponds to a medium dense liquid, which is due to the soft effective repulsive interactions rather weakly correlated[45]. Periodic boundary conditions and the minimum image convention[41] are employed. The interaction range in the system is given by the range of the effective pair potential between molecules and the geometry of tetrahedral molecules, i.e., the most outer atoms of two tetrahedral molecules with centers of mass slightly less than  $2.31\sigma$  apart still experience the effective potential contribution in Eq. (19). Hence, the actual interaction range in the system is approximately  $3.5\sigma$ .

All molecules are initially randomly placed in a cubic box of size  $a = 36.845\sigma$ . To remove the overlaps between them, a  $50\tau$  long warm-up run is performed during which the repulsive interparticle potential is capped (see capped interactions in Ref. [46]). Thus, at all interparticle distances, which would lead to larger forces between particles than a prescribed maximal force, the forces defined by the original repulsive pair potential are replaced by repulsive central forces of the maximal force magnitude. The latter is gradually increased from  $20\varepsilon/\sigma$  to  $110\varepsilon/\sigma$  during this warm-up phase. Afterwards an additional  $250\tau$  equilibration run is carried out where we set the maximal force magnitude to  $10^9\varepsilon/\sigma$ , which corresponds to interparticle distance of  $0.27\sigma$ . The chosen maximal force magnitude value is so high that it has no effect on the dynamics of molecules in the atomistic region because there atoms never come this close together. Therefore, by this force capping we only prevent possible force singularities that could emerge due to overlaps with the neighboring molecules when a given molecule enters the interface layer from



the coarse-grained side as explained in the previous section. Production runs with the  $10^9 \varepsilon / \sigma$  force capping are then performed for  $7500\tau$ , storing configurations at each  $5\tau$  time interval for analysis. We performed all our MD simulations using the ESPResSo package[46], developed at our institute.

The following reduced Lennard-Jones units[41] are used throughout:  $m^* = m/m_0$ ,  $r^* = r/\sigma$ ,  $V^* = V/\sigma^3$ ,  $T^* = k_B T/\varepsilon$ ,  $U^* = U/\varepsilon$ ,  $p^* = p\sigma^3/\varepsilon$ ,  $\rho^* = n/V^*$ ,  $t^* = t/\tau$ ,  $D^* = D\sqrt{m_0/\varepsilon}/\sigma$ , where  $D$  is the self-diffusion constant. Note that in our simulations all atoms have a mass  $m^* = 1$  while all molecules have a mass  $M^* = 4$ .

## IV. RESULTS AND DISCUSSION

### Determination of the Effective Potential

We have determined the effective nonbonded pair potential  $U^{cm*}$  between coarse-grained molecules illustrated in figure 3 by using the potential of mean force (PMF<sub>ex</sub>) of the *ex* system, Eq. (3), at very low number density  $\rho^* = 0.0025$  as the initial guess. Then we further adjusted it to obtain the adequate agreement between RDF<sub>cm,s</sub> of the *ex* and *cg* systems at the  $\rho^* = 0.1$ . We have

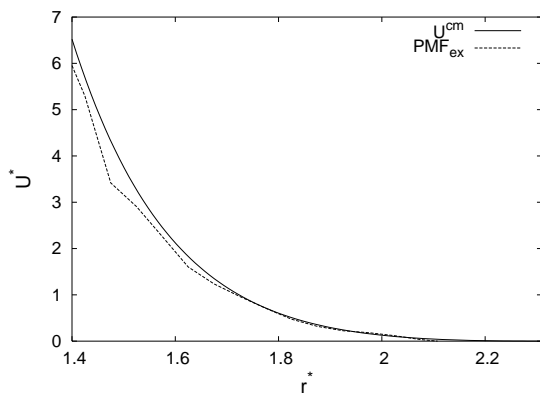


FIG. 3: The effective pair potential  $U^{cm*}$ , Eq. (22), between the coarse-grained molecules, where the potential of mean force PMF<sub>ex</sub> of the explicit system at  $\rho^* = 0.0025$  and  $T^* = 1$  was used as the initial guess. The presented function  $U^{cm*}$  was determined in such a way that the RDF<sub>cm,s</sub> of the explicit (*ex*) and coarse-grained (*cg*) systems match at the  $\rho^* = 0.1$ .

parameterized the effective potential  $U^{cm}$  with the Morse potential

$$U^{cm*}(r^*) = \gamma^* \{1 - \exp[-\kappa^*(r^* - r_0^*)]\}^2 \quad (22)$$

with parameters  $\gamma^* = \gamma/\varepsilon = 0.105$ ,  $\kappa^* = \kappa\sigma = 2.4$ , and  $r_0^* = r_0/\sigma = 2.31$ . As one can see from figure 3, the obtained effective potential is softer than the underlying repulsive interatomic interaction potential given by Eqs. (1) and (2) since it varies more slowly with the interparticle distance. This is a general feature of effective potentials for polyatomic molecular systems[33].

The obtained RDF<sub>cm,s</sub> of the *ex* and *cg* systems at the temperature  $T^* = 1$  and number density  $0.025 \leq \rho^* \leq 0.175$  using for all number densities the same effective potential given by Eq. (22) for the pair interactions between the coarse-grained molecules are depicted in figure 4. The

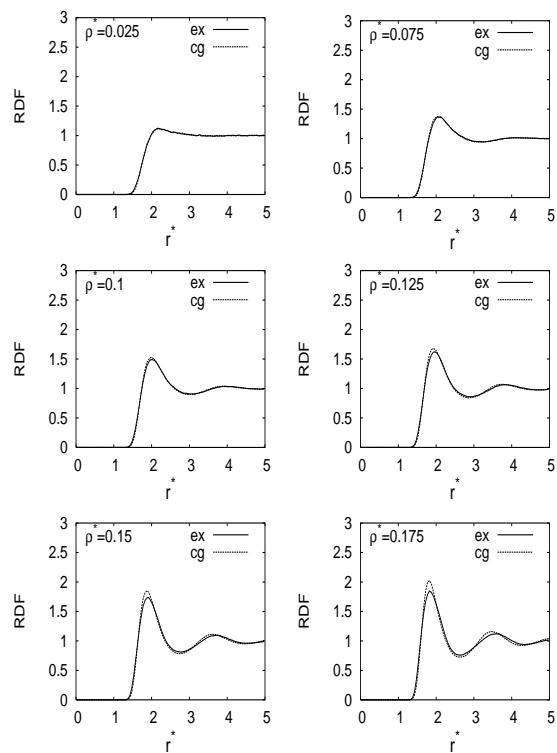


FIG. 4: Center-of-mass radial distribution functions of the explicit (*ex*) and coarse-grained (*cg*) systems at the temperature  $T^* = 1$  and number density  $0.025 \leq \rho^* \leq 2.25$ .

RDF<sub>cm,s</sub> are calculated in the range  $r^* \in [0, 5]$  with  $\Delta r^* = 0.05$ . From results presented in figure 4 it can be observed that although the effective potential given by Eq. (22) was parameterized at the number density  $\rho^* = 0.1$  the agreement of RDF<sub>cm,s</sub> of the *cg* system with the corresponding reference RDF<sub>cm,s</sub> of the *ex* system is good also for the lower number densities. In fact, due to weaker many-body interactions the agreement is even bet-

ter for the systems with lower density. Since the effective potentials are density dependent[31], to obtain a better agreement for higher densities the effective potential should be reparameterized[34]. Probably the functional form of the effective potential will also change due to increased contribution from many-body interactions.

As a quantitative measure of accuracy of the evaluated  $\text{RDF}_{cm}$ s we define a penalty function  $f_p$  as

$$f_p = \int [g(r^*) - g_{ex}^{cm}(r^*)]^2 \exp(-r^*) dr^*, \quad (23)$$

where  $g_{ex}^{cm}$ , which is taken as a reference, is the  $\text{RDF}_{cm}$  of the *ex* system. The function  $\exp(-r^*)$  is employed to penalize more strongly deviations at small distances[34]. The values of  $f_p$  for *cg* systems with the number density  $0.025 \leq \rho^* \leq 0.175$  are reported in table I. As expected the  $f_p$  grows with

$\rho^*$	$f_p \cdot 10^3$
0.025	0.0401
0.075	0.1101
0.1	0.2067
0.125	0.4361
0.150	0.9257
0.175	1.9025

TABLE I: Penalty function  $f_p$  defined by Eq. (23) as a function of number density  $\rho^*$  for  $\text{RDF}_{cm}$ s  $g_{cg}^{cm}(r^*)$  of the coarse-grained systems in which particles are interacting via the effective potential  $U^{cm*}$  given by Eq. (22). The  $\text{RDF}_{cm}$ s  $g_{ex}^{cm}(r^*)$  of all-atom systems at the corresponding  $\rho^*$  are taken for the reference  $\text{RDF}_{cm}$ s.

the growing density of the system.

From the  $\text{RDF}_{cm}$  we can evaluate the average number of neighbors of a given molecule within a sphere with the radius  $r^*$  as

$$n_n(r^*) = \rho^* \int_0^{r^*} g(r^*) 4\pi r^{*2} dr^*. \quad (24)$$

The  $n_n(r^*)$  for the *ex* and *cg* systems at the temperature  $T^* = 1$  and number density  $0.025 \leq \rho^* \leq 0.175$  are shown in figure 5. Despite the deviations between the  $\text{RDF}_{cm}$ s of the *ex* and *cg* systems the corresponding average numbers of neighbors exactly match, indicating, together with the  $\text{RDF}_{cm}$ s presented in figure 4, that the *cg* model with the molecules interacting via the effective potential given by Eq. (22) reproduces well the structure of the underlying *ex* system.

To show that the *cg* system with the effective potential from Eq. (22) is at the same state point

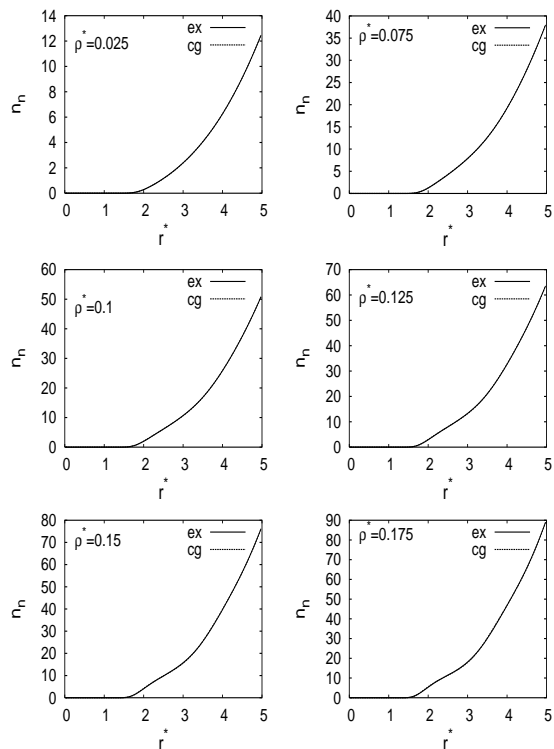


FIG. 5: The average number of neighbors  $n_n(r^*)$  of a given molecule as a function of distance for explicit (*ex*) and coarse-grained (*cg*) systems at the temperature  $T^* = 1$  and number density  $0.025 \leq \rho^* \leq 0.175$ .

as the original *ex* system at the same temperature and density we also evaluated the pressure in the system. The equations of state for the *ex* and *cg* models are shown in figure 6. The resulting

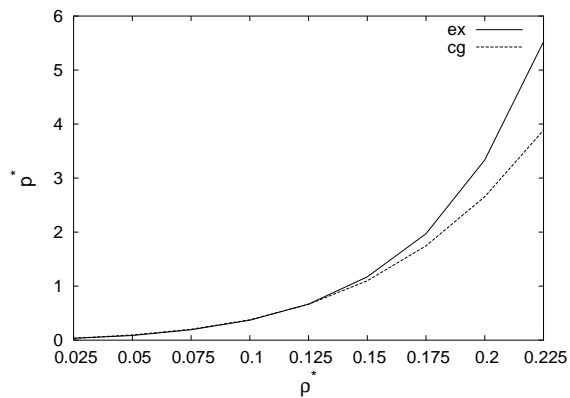


FIG. 6: Pressure  $p^*$  in the explicit (*ex*) and coarse-grained (*cg*) systems at the temperature  $T^* = 1$  as a function of the number density  $\rho^*$  of the system.

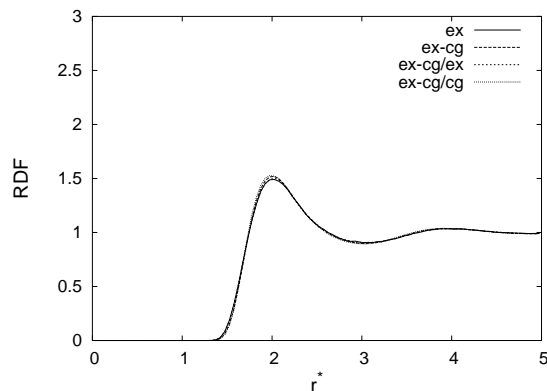
equations of state are similar to the case of colloidal sphere systems[35]. This similarity is to be expected since the tetrahedral molecule as well as the spherical coarse-grained molecule can be considered as spherical colloidal particles with a hard core and a soft coating layer. From figure 6 we can conclude that the *cg* model with the particles interacting via the effective potential from Eq. (22) reproduces the equation of state of the underlying *ex* system up to  $\rho^* = 0.125$ , at which the two pressure curves start deviating from each other, reflecting the fact that the effective potential is density dependent. In order to minimize the artifacts originating from our parameterization of the effective potential while still simulating the liquid state we have decided to perform all our MD simulations of the hybrid atomistic/mesoscopic (*ex-cg*) model at the state point with  $T^* = 1$  and density  $\rho^* = 0.1$ .

### Statistical Properties

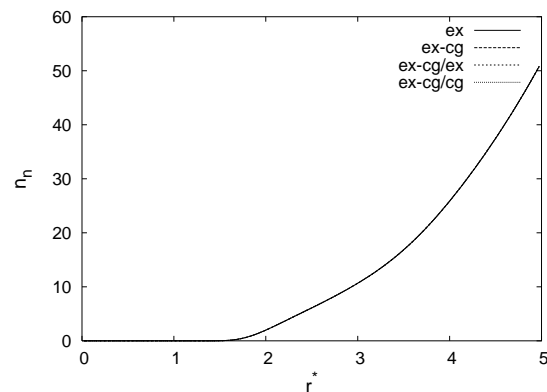
The new adaptive resolution scheme is tested by comparing the computed statistical properties of the *ex-cg* model with the corresponding properties of the reference fully atomistic *ex* system.

Figure 7 (a) displays the  $\text{RDF}_{cm}$ s calculated from center-of-mass positions of all molecules in the box of the *ex* and *ex-cg* systems at  $\rho^* = 0.1$  and  $T^* = 1$ . Shown is the case with the width of the interface layer  $2d^* = 2.5$ . Depicted are also the corresponding local  $\text{RDF}_{cm}$ s for the explicit (*ex-cg/ex*) and coarse-grained regions (*ex-cg/cg*) of the *ex-cg* model. As in all simple liquids, e.g., methane, the  $\text{RDF}_{cm}$ s are zero at short distances between molecules' centers of mass because repulsive forces prevent overlapping of molecules. Then the functions increase rapidly to the first peak. With increasing distance  $\text{RDF}_{cm}$ s reach the limiting value 1 after few oscillations, indicating that there is no order at long distances. The average numbers of neighbors  $n_n(r^*)$  of a given molecule as functions of distance are illustrated in figure 7 (b). The number of nearest neighbors in the first layer corresponding to the first minimum in the  $\text{RDF}_{cm}$  is about 11. For comparison, the corresponding experimental value from X-ray diffraction for liquid methane at  $T = 92$  K is approximately 12[47].

All calculated  $\text{RDF}_{cm}$ s of the *ex-cg* model and  $n_n(r^*)$  are in good agreement with the reference  $\text{RDF}_{cm}$  and  $n_n(r^*)$  of the *ex* model indicating that the structure of the underlying all-atom system is well reproduced using the adaptive resolution



(a)



(b)

FIG. 7: (a) Center-of-mass radial distribution functions for all molecules in the box of the all-atom (*ex*) and hybrid atomistic/mesoscopic (*ex-cg*) systems at  $\rho^* = 0.1$  and  $T^* = 1$ . Shown are also the corresponding center-of-mass radial distribution functions for only the explicit molecules from the explicit region (*ex-cg/ex*) and for only the coarse-grained molecules from the coarse-grained region (*ex-cg/cg*). The width of the interface layer is  $2d^* = 2.5$ . (b) The corresponding average numbers of neighbors  $n_n(r^*)$  of a given molecule as functions of distance. The different curves are almost indistinguishable.

scheme. This is further confirmed by the values of the penalty function  $f_p$  reported in table II, evaluated for different interface layer widths. From the results given in table II we can see that the local structure in the explicit region of the *ex-cg* model is exactly reproduced independently of the interface layer width. In contrast, the accuracy of the

$2d^*$	$f_p \cdot 10^3$		
	ex-cg	ex-cg/ex	ex-cg/cg
2.5	0.0821	0.0009	0.2109
3.0	0.0893	0.0008	0.2158
4.0	0.1058	0.0016	0.2197
5.0	0.1324	0.0023	0.2315
6.0	0.1583	0.0033	0.2367
7.0	0.1944	0.0047	0.2449
8.0	0.2301	0.0076	0.2616
9.0	0.2695	0.0082	0.2489
10.0	0.3159	0.0101	0.2632

TABLE II: Penalty function  $f_p$  defined by Eq. (23) as a function of the interface layer width  $2d^*$  for RDF $_{cm}$ s  $g_{ex-cg}^{cm}(r^*)$ ,  $g_{ex-cg/ex}^{cm}(r^*)$ ,  $g_{ex-cg/cg}^{cm}(r^*)$  of the hybrid atomistic/mesoscopic model at  $\rho^* = 0.1$  and  $T^* = 1$ .  $g_{ex-cg}^{cm}(r^*)$  is the RDF $_{cm}$  of all molecules in the box where all molecules are considered indistinguishable,  $g_{ex-cg/ex}^{cm}(r^*)$  is the RDF $_{cm}$  of only the explicit molecules from the explicit region while  $g_{ex-cg/cg}^{cm}(r^*)$  is the RDF $_{cm}$  of only the coarse-grained molecules from the coarse-grained region. The RDF $_{cm}$   $g_{ex}^{cm}(r^*)$  of all-atom system at the corresponding  $\rho^*$  and  $T^*$  is taken for the reference RDF $_{cm}$ .

local structure reproduction in the coarse-grained region of the *ex-cg* model depends on the accuracy of the effective potential parameterization in the *cg* model (see the value of  $f_p$  given in table I for  $\rho^* = 0.1$ ). The computed  $f_p$ s for the total RDF $_{cm}$  of the *ex-cg* model lie up to  $2d^* = 8.0$  in between the values for the local explicit and coarse-grained RDF $_{cm}$ s.

For narrow interface layers with  $2d^* < 2.5$  the adaptive resolution scheme fails to work. The molecules are not given enough space and time to adapt their orientation to their environment and the system is not properly equilibrated in this case. The value  $2d^* = 2.5$ , for which the adaptive resolution scheme gives the acceptable results, can be rationalized by the fact that the interface layer width should at least exceed the maximal range of interaction, which is the range of the effective potential, namely  $2.31\sigma$ .

To demonstrate that the thermodynamic properties are correctly reproduced by the adaptive resolution scheme the temperature and pressure of the system as a functions of the interface layer width are given in tables III and IV, respectively. The calculated temperature profile reported in table III shows that the system is at the right temperature and that all degrees of freedom are properly equilibrated in accordance with the equipartition principle regardless of the interface layer width. The results given in table IV also show

that the adaptive resolution scheme succeeds in reproducing the pressure of the underlying fully atomistic system.

In order to check that the chemical potentials in the atomistic and coarse-grained regions are equal as required by the condition (4) we report in table V the average number of molecules in different regions of the system. In table V we also give the number of degrees of freedom  $n_{DOF}$  in the system defined as

$$n_{DOF} = 3 \sum_{\alpha} [w_{\alpha} N + (1 - w_{\alpha})], \quad (25)$$

where  $N = 4$  is the number of explicit tetrahedral atoms in a molecule and  $w_{\alpha}$  is the value of the weighting function defined by Eq. (11) for the molecule  $\alpha$ . The summation in Eq. (25) goes over all  $n$  molecules of the system. The results show that there is no molecule number bias in the system and that the *ex-cg* system is homogeneous. Note that  $n_{DOF}$  is greatly reduced employing the adaptive resolution scheme on the *ex-cg* model in comparison with the fully atomistic model. The time evolution of the number of molecules in different regions of the system together with the  $n_{DOF}$  is illustrated in figure 8. The results clearly

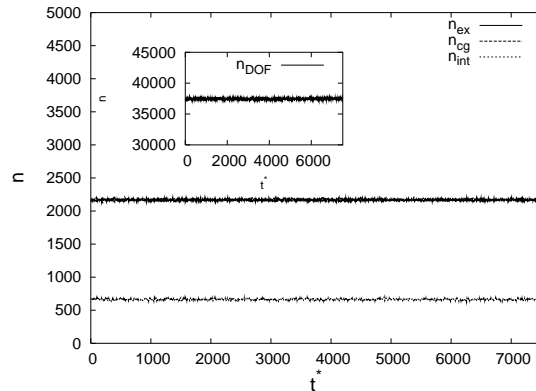


FIG. 8: Time evolution of number of molecules in a explicit ( $n_{ex}$ ), coarse-grained ( $n_{cg}$ ), and interface regions ( $n_{int}$ ) in the hybrid atomistic/mesoscopic model with the  $2.5\sigma$  interface layer width. Time evolution of number of degrees of freedom in the system ( $n_{DOF}$ ) is depicted in the inset.

demonstrate that the system is in thermodynamical equilibrium, indicating that the conditions (4) are satisfied by our adaptive resolution scheme.

Although we have parameterized the effective potential to reproduce the structural properties of the *ex* system we can also compare the dynamical properties of the *ex-cg* with the *ex* model. For

$2d^*$	$T$	$T_{ex}$	$T_{cg}$	$T_{int}$	$T_{ex}^{all}$	$T_{int}^{all}$
$0^{ex}$	$1.00 \pm 0.01$	$1.00 \pm 0.01$	—	—	$1.00 \pm 0.01$	—
$0^{cg}$	$1.00 \pm 0.01$	—	$1.00 \pm 0.01$	—	—	—
2.5	$1.00 \pm 0.01$	$1.00 \pm 0.01$	$1.00 \pm 0.02$	$1.00 \pm 0.03$	$1.00 \pm 0.01$	$1.00 \pm 0.02$
3.0	$1.00 \pm 0.01$	$1.00 \pm 0.02$	$1.00 \pm 0.02$	$1.00 \pm 0.03$	$1.00 \pm 0.01$	$1.00 \pm 0.02$
4.0	$1.00 \pm 0.01$	$1.00 \pm 0.01$	$1.00 \pm 0.02$	$1.00 \pm 0.03$	$1.00 \pm 0.01$	$1.00 \pm 0.01$
5.0	$1.00 \pm 0.01$	$1.00 \pm 0.02$	$1.00 \pm 0.02$	$1.00 \pm 0.02$	$1.00 \pm 0.01$	$1.00 \pm 0.02$
6.0	$1.00 \pm 0.01$	$1.00 \pm 0.02$	$1.00 \pm 0.02$	$1.00 \pm 0.02$	$1.00 \pm 0.02$	$1.00 \pm 0.02$
7.0	$1.00 \pm 0.01$	$1.00 \pm 0.02$	$1.00 \pm 0.02$	$1.00 \pm 0.02$	$1.00 \pm 0.02$	$1.00 \pm 0.01$
8.0	$1.00 \pm 0.01$	$1.00 \pm 0.02$	$1.00 \pm 0.02$	$1.00 \pm 0.02$	$1.00 \pm 0.02$	$1.00 \pm 0.01$
9.0	$1.00 \pm 0.01$	$1.00 \pm 0.03$	$1.00 \pm 0.03$	$1.00 \pm 0.02$	$1.00 \pm 0.01$	$1.00 \pm 0.01$
10.0	$1.00 \pm 0.01$	$1.00 \pm 0.03$	$1.00 \pm 0.02$	$1.00 \pm 0.02$	$1.00 \pm 0.01$	$1.00 \pm 0.02$

TABLE III: Average temperature as a function of the interface layer width  $2d^*$ .  $T$ ,  $T_{ex}$ ,  $T_{cg}$ , and  $T_{int}$  are the average temperatures of the total system, the explicit, coarse-grained, and interface layer regions, respectively, calculated by Eq. (17).  $T_{ex}^{all}$  and  $T_{int}^{all}$  are the average temperatures of the explicit and interface layer regions, respectively, calculated from total velocities (translational+vibrational+rotational) of explicit atoms in molecules.  $0^{ex}$  and  $0^{cg}$  denote the all-atom and coarse-grained systems, respectively.

$2d^*$	$p^*$
$0^{ex}$	$0.379 \pm 0.009$
$0^{cg}$	$0.378 \pm 0.004$
2.5	$0.382 \pm 0.007$
3.0	$0.383 \pm 0.006$
4.0	$0.384 \pm 0.006$
5.0	$0.385 \pm 0.007$
6.0	$0.386 \pm 0.006$
7.0	$0.388 \pm 0.004$
8.0	$0.389 \pm 0.006$
9.0	$0.390 \pm 0.005$
10.0	$0.391 \pm 0.006$

TABLE IV: Average pressure calculated using Eq. (18) as a function of the interface layer width  $2d^*$ .  $0^{ex}$  and  $0^{cg}$  denote the all-atom and coarse-grained systems, respectively.

that purpose we have computed the self-diffusion coefficient, which is evaluated from the center-of-mass displacements using the Einstein relation

$$D^* = \frac{1}{6} \lim_{t^* \rightarrow \infty} \frac{\langle |\mathbf{R}_\alpha^*(t^*) - \mathbf{R}_\alpha^*(0)|^2 \rangle}{t^*}, \quad (26)$$

where  $\mathbf{R}_\alpha^*(t^*)$  is the center-of-mass position of the molecule  $\alpha$  at time  $t^*$  and averaging is performed over all molecules and all choices of time origin. The self-diffusion coefficient of the  $ex$  and  $cg$  models calculated in the microcanonical ensemble, where the Langevin thermostat is switched off after the initial warm-up run, are 0.24 and 0.30, respectively. The corresponding values of the self-diffusion coefficient for the  $ex$ ,  $cg$ , and  $ex$ - $cg$  models with the Langevin thermostat switched on are 0.12, 0.14, and 0.13, respectively. Since we use the same time and length scales in all our three mod-

$2d^*$	$n_{ex}$	$n_{cg}$	$n_{int}$	$n_{DOF}$
$0^{ex}$	5001	0	0	60012
$0^{cg}$	0	5001	0	15003
2.5	$2167 \pm 38$	$2170 \pm 48$	$663 \pm 21$	$37446 \pm 516$
3.0	$2100 \pm 45$	$2103 \pm 60$	$796 \pm 37$	$37455 \pm 493$
4.0	$1966 \pm 58$	$1969 \pm 47$	$1064 \pm 40$	$37467 \pm 507$
5.0	$1832 \pm 47$	$1835 \pm 56$	$1332 \pm 43$	$37470 \pm 501$
6.0	$1697 \pm 57$	$1701 \pm 54$	$1601 \pm 34$	$37467 \pm 330$
7.0	$1563 \pm 45$	$1566 \pm 29$	$1871 \pm 31$	$37479 \pm 526$
8.0	$1428 \pm 48$	$1431 \pm 27$	$2141 \pm 22$	$37479 \pm 345$
9.0	$1294 \pm 22$	$1295 \pm 23$	$2411 \pm 60$	$37488 \pm 576$
10.0	$1158 \pm 33$	$1160 \pm 16$	$2682 \pm 56$	$37482 \pm 63$

TABLE V: Average number of molecules as a function of the interface layer width  $2d^*$ .  $n_{ex}$ ,  $n_{cg}$ , and  $n_{int}$  are the average number of molecules in the explicit, coarse-grained, and interface layer regions, respectively.  $n_{DOF}$  is the average number of degrees of freedom defined by Eq. (25). For orientation: in the system with 2500 coarse-grained molecules, 2500 four atom explicit molecules, and no hybrid molecules  $n_{DOF} = 37500$ .  $0^{ex}$  and  $0^{cg}$  denote the all-atom and coarse-grained systems, respectively.

els different values of the self-diffusion coefficient in the  $ex$  and  $cg$  models (with no Langevin thermostat applied) indicate that the coarse-grained molecules experience a slightly smaller intermolecular frictional hindrance in their motion compared to the explicit molecules. This indicates that the effective pair potential given in Eq. (22) introduces an effective time scale shift in the coarse-grained regime. This is known from other studies [16, 17], where one actually takes advantage of that in order to reach very long simulation times[48]. The apparent self-diffusion coefficient values of the

*ex* and *cg* models are lower and much closer together when the Langevin thermostat is applied due to the frictional forces arising from the coupling to the thermostat unlike to the case of polymers. There typically the friction of the thermostat is negligible compared to the friction between monomers. Since the self-diffusion coefficient of the *ex-cg* model is close to the corresponding values for the *ex* and *cg* models we can conclude that the center-of-mass dynamics of the molecules is similar in all three models.

As the final test to demonstrate the reliability of the adaptive resolution scheme we have computed the number density profile of the *ex-cg* model. The results for the system with  $2d^* = 2.5$  and  $2d^* = 10.0$  are presented in figures 9 (a) and (b), respectively. The results in figure 9 (a) for the case of  $2d^* = 2.5$  show that the explicit and coarse-grained regions have the same homogeneous density as the reference system while the density in the transition regime undergoes an oscillation around the reference value  $\rho_0^* = 1.0$  with a magnitude of approximately  $0.05\rho_0^*$ . In the case of  $2d^* = 10.0$  (figure 9 (b)) a 5% drop in the density occurs in the transition regime, which is compensated by the slight increase of the density in the explicit and coarse-grained regions.

This artifact can be explained by considering the results displayed in figure 10 (a), where the pressure of the system containing only hybrid molecules as a function of the constant value of the weighting function  $w$  (corresponding to the situation in the interface layer) is illustrated. The pressure is increased in comparison to the pressure in the reference system. Clearly the increase is most prominent for the most 'artificial' case with  $w = 1/2$ , indicating that there still is a small 'pressure barrier' in the interface region causing the density dip. This is also evident from results in figure 10 (b), where the  $RDF_{cm}$  and the potential of mean force of the system with  $w = 1/2$  are shown. The effective potential in a system containing only hybrid molecules with constant value of the weighting function changes in comparison to the all-atom system. This means that the hybrid molecules in the interface layers of the *ex-cg* model experience too strong effective interaction leading to the pressure variations in the interface layer. Since the artifact occurs at constant values of  $w$  it is an artifact of the linear combination of forces in Eq. (7) and not of the functional form of the weighting function  $w$ . It must be emphasized, however, that this artifact of the proposed adaptive resolution scheme is within a 5% error and

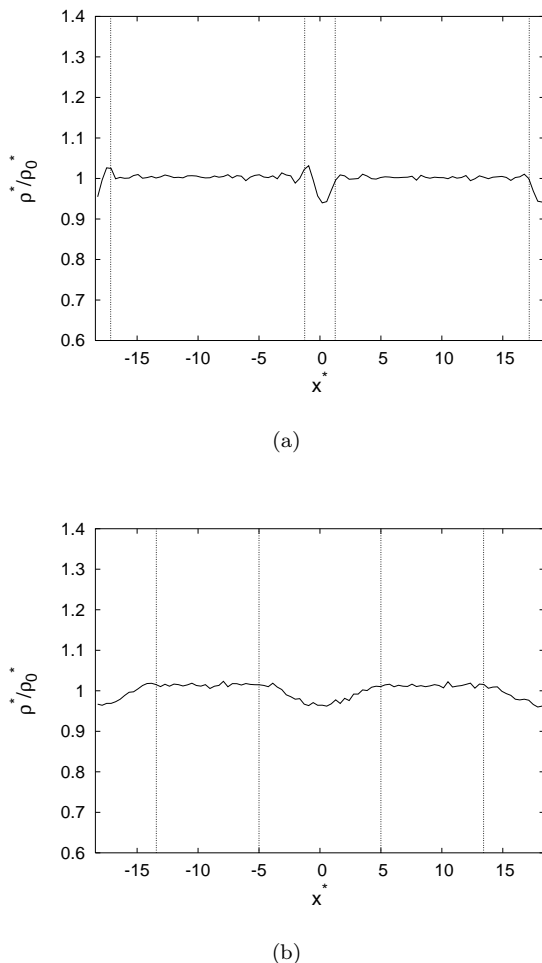
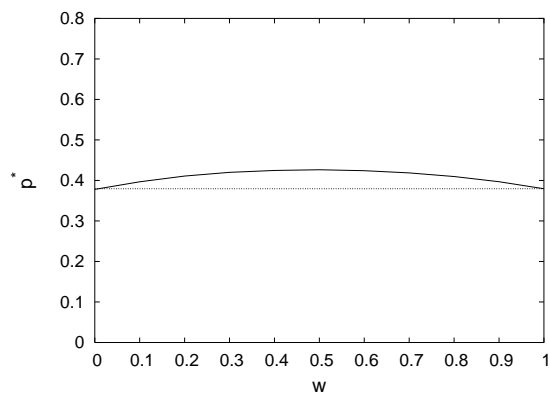


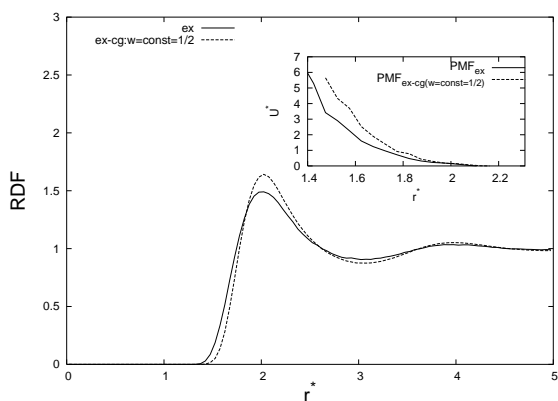
FIG. 9: (a) Normalized density profile in the  $x$  direction of the hybrid atomistic/mesoscopic model with the  $2.5\sigma$  interface layer width. Vertical lines denote boundaries between atomistic, coarse-grained and interface regions of the system. (b) The same as in (a) but for the  $10.0\sigma$  interface layer width.

that similar artifacts, occurring at the boundary of two domains with different level of detail, are also characteristic for other hybrid schemes[49].

The pressure variations in the interface layer could cause a spurious reflection of molecules from the boundary. However, the results presented in figure 11, where the time evolution of two diffusion profiles is monitored for molecules that are initially localized at the two slabs with  $a^*/10$  width neighboring the interface layer, show that this is not the case. The molecules initially localized at the two slabs spread out symmetrically with time. This is because the self-diffusion coefficients of all



(a)



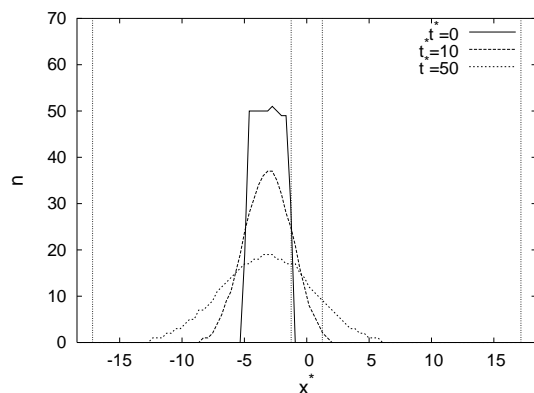
(b)

FIG. 10: Artifacts of the adaptive resolution scheme. (a) Average pressure  $p^*$  in the system containing only hybrid molecules as a function of the constant value of the weighting function  $w$ . (b) Center-of-mass radial distribution functions for the explicit system (ex) and the system containing only hybrid molecules with  $w = \text{const} = 1/2$  (ex-cg( $w=\text{const}=1/2$ )) at  $\rho^* = 0.0025$  and  $T^* = 1$ . The inset also shows the corresponding  $\text{PMF}_{\text{ex}}$  and  $\text{PMF}_{\text{ex-cg}(w=\text{const}=1/2)}$  determined from the systems with  $\rho^* = 0.0025$  using Eq. (3).

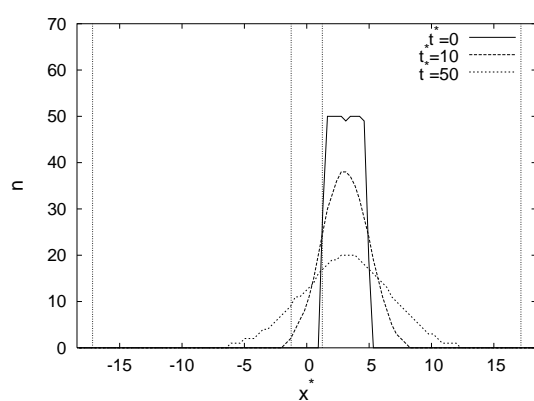
models are approximately the same in the case of the applied Langevin thermostat. Thus, the two distributions occupy at time  $t^*$  regions with mean square radius

$$\langle |x^*(t^*) - x^*(0)|^2 \rangle \simeq 2D^*t^*, \quad (27)$$

where  $x^*(0)$  is the center of the distribution at time  $t^* = 0$ , which is equal to  $-d^* - a^*/20$  for the left slab (figure 11 (a)) and  $d^* + a^*/20$  for



(a)



(b)

FIG. 11: Time evolution of diffusion profiles for the molecules that are initially, at time  $t^* = 0$ , localized at two neighboring slabs of the mid interface layer with  $2d^* = 2.5$  ( $n$  is the number of this molecules with the center-of-mass position at a given coordinate  $x^*$ ). The width of the two slabs is  $a^*/10$ . Vertical lines denote boundaries of the interface layer. (a) The diffusion profile, averaged over 500 different time origins, at  $t^* = 0$ ,  $t^* = 10$ , and  $t^* = 50$  for the molecules that are initially localized at the slab on the coarse-grained side of the interface region. (b) The same as in (a) but for the molecules that are initially localized at the slab on the atomistic side of the interface region.

the right slab (figure 11 (b)). Since the diffusion profiles are symmetrical at any given time we can conclude that the artifact at the interface layer is too small to have any severe effect on the diffusion of molecules across the interface layer.

## V. CONCLUSIONS

A novel approach for efficient hybrid atomistic/mesoscale molecular dynamics (MD) simulations has been presented in this paper. The new adaptive resolution MD simulation scheme dynamically couples the atomic and mesoscale length scales of the studied system by allowing an on-the-fly dynamical interchange between molecules' atomic and mesoscopic levels of description. In our approach the number of degrees of freedom is allowed to fluctuate during the course of simulation while the statistical properties of the underlying all-atom model are properly reproduced for both levels of detail. Since the purpose of this paper was to develop the method, we restricted ourselves to a most simple model system of a molecular liquid with short-range repulsive interactions. Even on this level a number of questions still have to be tackled, as there is the application to higher liquid densities for complex molecular liquids or the proper analysis and understanding of the time scale problem, when the diffusion on the coarse-grained level is faster than on the all-atom level. For separate runs at the two levels of detail this is understood, while the occurrence within one simulation box still poses some conceptual problems. On the other hand the current density is in between a typical small molecule liquid and a polymeric fluid. Thus we expect that already this approach can be generalized and applied to differ-

ent realistic soft condensed matter systems where both atomic and mesoscopic length scales have to be considered. This can be either polymer solutions and melts, such as a synthetic or biological macromolecule embedded in a solvent. Similarly our method should also find application for other polymer systems (same force field), molecular liquids such as methane (same geometry) or water (tetrahedral clusters), etc., enabling to reach much larger length and time scales than for all-atom MD simulations. In all cases the aim is to treat in a simulation only as many degrees of freedom as absolutely necessary for the question considered. In this sense the region of higher detail can be either given by a geometrical constraint, e.g., close to a surface, or even be chosen on demand due to specific local conformations of a (macro-)molecular system. Work along these lines is underway.

## ACKNOWLEDGMENTS

We thank A. Arnold, B. A. Mann, P. Schravendijk, B. Hess, and N. van der Vegt for useful discussions. We are also grateful to C. F. Abrams for discussions at early stage of this work. This work is supported in part by the Volkswagen foundation. M. P. acknowledges the support of the Ministry of Higher Education, Science and Technology of Slovenia under grant No. P1-0002.

- 
- [1] P. Deuffhard, J. Hermans, B. Leimkuhler, A. Mark, S. Reich and R. Skeel, editors, *Computational Molecular Dynamics: Challenges, Methods, Ideas*, volume 4 of *Lecture Notes in Computational Science and Engineering*, Springer Verlag, 1999.
  - [2] P. Minary, M. E. Tuckerman, and G. J. Martyna, *Phys. Rev. Lett.* **93**, 150201 (2004).
  - [3] D. Janežič, M. Praprotnik, and F. Merzel, *J. Chem. Phys.* **122**, 174101 (2005).
  - [4] M. Praprotnik and D. Janežič, *J. Chem. Phys.* **122**, 174102 (2005).
  - [5] M. Praprotnik and D. Janežič, *J. Chem. Phys.* **122**, 174103 (2005).
  - [6] M. Praprotnik, D. Janežič, and J. Mavri, *J. Phys. Chem. A* **108**, 11056 (2004).
  - [7] K. Kremer, and F. Müller-Plathe, *MRS Bulletin* **26**, 205 (2001).
  - [8] K. Kremer in "Multiscale Modelling and Simulation, Lecture Notes on Computational Science and Engineering, S. Attinger and P. Koumoutsakis eds, Springer 2004.
  - [9] G. S. Ayton, H. L. Tepper, D. T. Mirijanian, and G. A. Voth, *J. Chem. Phys.* **120**, 4074 (2004).
  - [10] M. Kranenburg, M. Venturoli, and B. Smit, *J. Phys. Chem. B* **107**, 11491 (2003).
  - [11] S. O. Nielsen, C. F. Lopez, G. Srinivas, and M. L. Klein, *J. Phys.: Condens. Matter* **16**, R481 (2004).
  - [12] S. J. Marrink, A. H. de Vries, and A. E. Mark, *J. Phys. Chem. B* **108**, 750 (2004).
  - [13] R. Chang, G. S. Ayton, and G. A. Voth, *J. Chem. Phys.* **122**, 244716 (2005).
  - [14] I. R. Cooke, K. Kremer, and M. Deserno, *Phys. Rev. E* **72**, 011506 (2005).
  - [15] K. Kremer and G. S. Grest, *J. Chem. Phys.* **92**, 5057 (1990).
  - [16] W. Tschöp, K. Kremer, J. Batoulis, T. Bürger, and O. Hahn, *Acta Polym.* **49**, 61 (1998).
  - [17] W. Tschöp, K. Kremer, O. Hahn, J. Batoulis, and T. Bürger, *Acta Polym.* **49**, 75 (1998).
  - [18] R. Everaers, S. K. Sukumaran, G. S. Grest, C. Svaneborg, A. Sivasubramanian, and K. Kre-



- mer, *Science* **303**, 823 (2004).
- [19] H. M. Chun, C. E. Padilla, D. N. Chin, M. Watanabe, V. I. Karlov, H. E. Alper, K. Soosaar, K. B. Blair, O. M. Becker, L. S. D. Caves, R. Nagle, D. N. Haneym, and B. L. Farmer, *J. Comput. Chem.* **21**, 159 (2000).
- [20] A. Malevanets and R. Kapral, *J. Chem. Phys.* **112**, 7260 (2000).
- [21] E. Villa, A. Balaeff, and K. Schulten, *PNAS* **102**, 6783 (2005).
- [22] L. Delle Site, C. F. Abrams, A. Alavi, and K. Kremer, *Phys. Rev. Lett.* **89**, 156103 (2002).
- [23] C. F. Abrams, L. Delle Site, and K. Kremer, *Phys. Rev. E* **67**, 021807 (2003).
- [24] L. Delle Site, S. Leon, and K. Kremer, *J. Am. Chem. Soc.* **126**, 2944 (2004).
- [25] A. Laio, J. VandeVondele and U. Roethlisberger, *J. Chem. Phys.* **116**, 6941 (2002).
- [26] H. Rafii-Tabar, L. Hua, and M. Cross, *J. Phys.: Condens. Matter* **10**, 2375 (1998).
- [27] J. Q. Broughton, F. F. Abraham, N. B. Bernstein, and E. Kaxiras, *Phys. Rev. B* **60**, 2391 (1999).
- [28] J. A. Smirnova, L. V. Zhigilei, and B. J. Garrison, *Comp. Phys. Commun.* **118**, 11 (1999).
- [29] G. Csanyi, T. Albaret, M. C. Payne, and A. D. Vita, *Phys. Rev. Lett.* **93**, 175503 (2004).
- [30] C. F. Abrams, Inhomogenous coarse-graining of polymers and polymer/metal interfaces, in *Computational Soft Matter: From Synthetic Polymers to Proteins*, edited by N. Attig, K. Binder, H. Grubmüller, and K. Kremer, volume 23 of *NIC Series*, pages 275–288, John von Neumann Institute for Computing, 2004.
- [31] A. A. Louis, *J. Phys.: Condens. Matter* **14**, 9187 (2002).
- [32] S. Curtarolo and G. Ceder, *Phys. Rev. Lett.* **88**, 255504 (2002).
- [33] S. H. L. Klapp, D. J. Diestler, and M. Schoen, *J. Phys.: Condens. Matter* **16**, 7331 (2004).
- [34] D. Reith, M. Pütz, and F. Müller-Plathe, *J. Comput. Chem.* **24**, 1624 (2003).
- [35] G. Bryant, S. R. Williams, L. Qian, I. K. Snook, E. Perez, and F. Pincet, *Phys. Rev. E* **66**, 060501(R) (2002).
- [36] C. P. Lawrence and J. L. Skinner, *Chem. Phys. Lett.* **372**, 842 (2003).
- [37] R. W. Zwanzig, *J. Chem. Phys.* **22**, 1420 (1954).
- [38] A. R. Leach, *Molecular Modelling*, Pearson Education Limited, Harlow, 2 edition, 2001.
- [39] F. Schwabl, *Quantum Mechanics*, Springer-Verlag, Berlin Heidelberg, 2 edition, 1996.
- [40] T. Soddemann, B. Dünweg, and K. Kremer, *Phys. Rev. E* **68**, 046702 (2003).
- [41] M. P. Allen and D. J. Tildesley, *Computer Simulation of Liquids*, Clarendon Press, Oxford, 1987.
- [42] H. Berendsen, J. Postma, W. V. Gunsteren, A. D. Nola, and J. Haak, *J. Chem. Phys.* **81**, 3684 (1984).
- [43] B. A. Mann, R. Everaers, C. Holm, and K. Kremer, *Europhys. Lett.* **67**, 786 (2004).
- [44] B. Dünweg and W. Paul, *Int. J. Mod. Phys. C* **2**, 817 (1991).
- [45] The physically correct way of course would be to calculate the second virial coefficient. This here is not that helpful, because the interaction potential is rather smooth. The present measure is more appropriate, when the structure of the liquids is compared in an NVT simulation, as in our case.
- [46] <http://www.espresso.mpg.de>.
- [47] A. Habenschuss, E. Johnson, and A. H. Narten, *J. Chem. Phys.* **74**, 5234 (1981).
- [48] S. Leon, N. van der Vegt, L. Delle Site, and K. Kremer, *Macromolecules* in press (2005).
- [49] W. Cai, M. de Koning, V. V. Bulatov, and S. Yip, *Phys. Rev. Lett.* **85**, 3213 (2000).